ACS APPLIED MATERIALS & INTERFACES

Research Article

Cite This: ACS Appl. Mater. Interfaces 2019, 11, 12880−12889

www.acsami.org

Ecofriendly Electrospun Membranes Loaded with Visible-Light-Responding Nanoparticles for Multifunctional Usages: Highly Efficient Air Filtration, Dye Scavenging, and Bactericidal Activity

Dan Lv,[†] Ruoxue Wang,[†] Guosheng Tang,[†] Zhipeng Mou,[†] Jiandu Lei,[⊥] Jingquan Han,[‡] Stefaan De Smedt,[†,∥] Ranhua Xiong,*[,†] and Chaobo Huang*[,†,§]

[†]College of Chemical Engineering, Key Laboratory of Forestry Genetics & Biotechnology, Ministry of Education, [‡]College of Materials Science and Engineering, and [§]Laboratory of Biopolymer based Functional Materials, Jiangsu Co-Innovation Center of Efficient Processing and Utilization of Forest Resources, Nanjing Forestry University (NFU), Nanjing 210037, P. R. China

[∥]Lab General Biochemistry & Physical Pharmacy, Department of Pharmaceutics, Ghent University, Ghent 9000, Belgium

[⊥]Beijing Key Laboratory of Lignocellulosic Chemistry, and MOE Engineering Research Center of Forestry Biomass Materials and Bioenergy, Beijing Forestry University, Beijing 100083, P. R. China

Supporting Information

ABSTRACT: Ambient particulate matter pollution has posed serious threats to global environment and public health. However, highly efficient filtration of submicron particles, the so-named "secondary pollution" caused by, e.g., bacterial growth in filters and the use of nondegradable filter materials, remains a serious challenge. In this study, poly(vinyl alcohol) (PVA) and konjac glucomannan (KGM)-based nanofiber membranes, loaded with ZnO nanoparticles, were prepared through green electrospinning and ecofriendly thermal cross-linking. Thus obtained fibrous membranes not only show highly efficient air-filtration performance but also show superior photocatalytic activity and antibacterial activity. The filtration efficiency of the ZnO@PVA/KGM membranes for ultrafine particles (300 nm) was higher than 99.99%, being superior to that of commercial HEPA filters. By virtue of the high photocatalytic activity, methyl orange was efficiently decolorized with a removal efficiency of more than 98% at an initial concentration of 20 mg L^{-1} under 120 min of solar irradiation. A multifunctional membrane with high removal efficiency, low flow resistance, superior photocatalytic activity, and superior antibacterial activity was successfully achieved. It is conceivable that the combination of a biodegradable polymer and an active metal particle would form an unprecedented photocatalytic system, which will be quite promising for environmental remediation such as air filtration and water treatment.

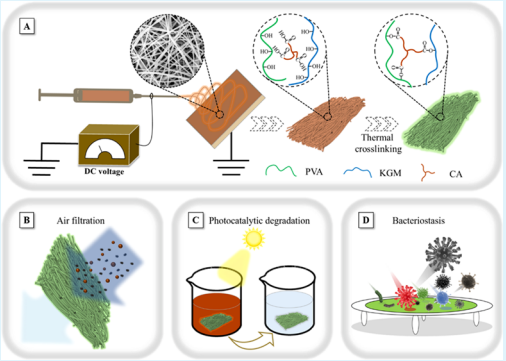

KEYWORDS: *air filtration, antibacterial, electrospinning nanofibers, multifunctional, photodegradation*

1. INTRODUCTION

Air pollution is an unvisitable killer. According to reports of the World Health Organization, most air pollution-related deaths are from noncommunicable diseases.[1] Indeed, air pollution contributes to stroke, lung cancer, chronic obstructive pulmonary disease, and ischemic heart disease.[1] In addition to the serious effect on human health, particulate matters (PMs) also affect the living environment like visibility that might contribute to climate change, etc.[2−5] It all explains why advanced filtering techniques to efficiently remove PMs from air are highly desirable.

Fibrous filters such as glass fibers, spun-bonded fibers, and melt-blown fibers are widely used in various air filtration devices. However, such fibrous filters usually show low filtration efficiency for fine (submicron) nanoparticles. This suboptimal filtration performance can be ascribed to the relatively large pores present in such filters, which is due to the use of micrometer-sized fibers, which may usually show poor uniformity (e.g., low control over the fiber diameter) and low mechanical performance.[6] Nanofiber membranes, made through electrospinning, were introduced to effectively resolve the filtration problems seen for ultrafine particles by virtue of the excellent advantages like a small diameter of the fiber, a controllable porous structure, a high specific surface area, good internal connectivity, and steerable morphology.[7−9] To date, various polymers have been successfully fabricated into nanofibrous membranes via electrospinning and evaluated for air filtration, like polyacrylonitrile,[8] polyethylene oxide,[10] polyurethane,[11] poly(vinyl alcohol) (PVA),[12] polysulfone,[10,13] poly(lactic acid),[14] polycarbonate,[15] polyamide,[7] and poly-

Received: January 23, 2019
Accepted: March 14, 2019
Published: March 14, 2019

DOI: 10.1021/acsami.9b01508
ACS Appl. Mater. Interfaces 2019, 11, 12880−12889

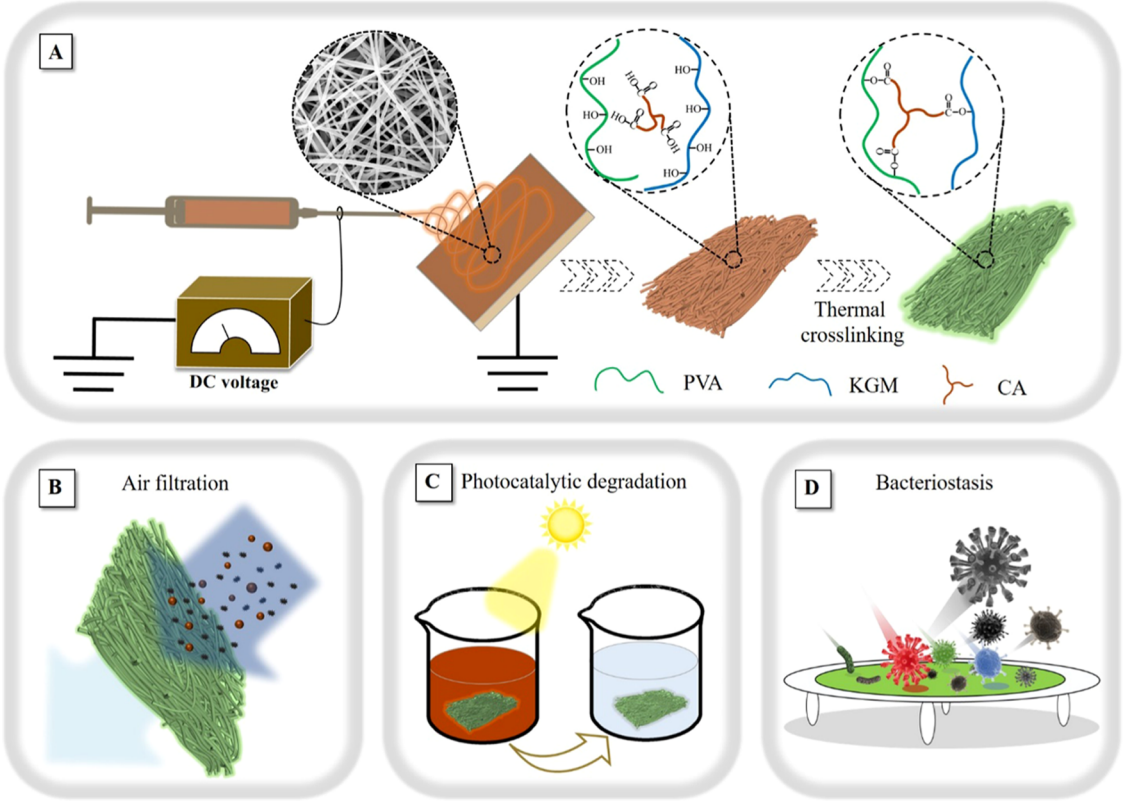

Figure 1. Multifunctional ZnO@PVA/KGM electrospun nanofiber membranes. (a) Schematic presentation of the preparation of the membranes by electrospinning and (b) their application for air filtration. (c) Photocatalytic degradation. (d) Antibacterial activity of the membranes.

imide.[16] Most of these electrospun polymer membranes possess superior filtration performance for ultrathin particulate contaminants. However, the so-named "secondary pollution", like bacterial growth in the membranes, restricts their use in practical applications. Also, and importantly, fully biodegradable electrospun polymer membranes are needed, taking into account the immense challenge the world faces from the so-named 'white pollution', referring to the accumulation of plastics in the environment. As Figure 1 illustrates, multifunctional ecofriendly electrospun polymer membranes with a sufficient thickness, to guarantee sufficiently high filtration efficiency, are needed. However, thicker membranes inevitably result in a higher pressure drop over the filter, which means a higher energy cost to filter air. To overcome these shortcomings, researchers have been looking for innovative strategies in recent years, for example, the exploitation of green chemistry to make electrospun nanofiber membranes,[17−20] the use of bio-originated and biodegradable polymers, and also the use of nanofiber membranes that are loaded with active components.[21−25]

Inspired by the earlier work, the natural polymer konjac glucomannan (KGM) and active metal oxide ZnO nanoparticles were induced with a water-soluble polymer PVA to form a uniform electrospun nanofiber membrane. As pure PVA and KGM nanofibers immediately dissolved upon contact with water, which seriously restricted their application, citric acid (CA) was introduced as the cross-linking agent to improve their mechanical properties. Compared with synthetic polymers, natural polymers are readily available, biocompatible, and biodegradable. KGM, as the natural polysaccharide, is well known to have more efficient physical and chemical properties, such as good water absorption and film-forming ability, as well as bioactivity.[26,27] To enhance the performance of the composite membrane and accord more functions, the incorporation of metal oxides was proposed earlier by our group.[12] Among existing active metal oxides, ZnO is a nearly ideal material in terms of the optical, electrical, chemical, and biological properties.[28] For that purpose, nanosized ZnO is an ideal metal oxide as it is biocompatible and also shows photocatalytic and antibacterial activities.[29,30] Indeed, as, e.g., industrial waste water is often polluted with organic dyes, it is highly desirable to degrade these refractory organics.[31] In the present work, a biocompatible and biodegradable blend of PVA and KGM electrospun nanofibrous membranes loaded with active ZnO nanoparticles (ZnO@PVA/KGM) was successfully prepared via green electrospinning and ecofriendly thermal cross-linking (Figure 1a). Thus, it is conceivable that the combination of electrospun-synthesized nanofibrous membranes and the photoactive nano-ZnO particles would form an unprecedented photocatalytic system with specific functions for air filtration (Figure 1b), photodegradation (Figure 1c), and bacteriostasis (Figure 1d).

2. EXPERIMENTAL METHODS

2.1. Materials. Poly(vinyl alcohol) (PVA-124, 98−99.8% hydrolyzed), agar powder, and beef extract were purchased from Sinopharm Chemical Reagent Co., Ltd., China. Konjac glucomannan (KGM, Mw ~900 000, 95%) was obtained from Jiangsu Boyao Bio-tech Co., Ltd. (Jiangsu, China), and zinc oxide (ZnO, 30 ± 10 nm) was purchased from Shanghai Macklin Biochemical Co., Ltd. Citric acid (CA, GR 99.8%) was purchased from Aladdin (Shanghai, China). Peptone was supplied by Beijing Aoboxing Bio-tech Co., Ltd., (Beijing, China). Sodium chloride was purchased from Xilong Chemical Co., Ltd., China. All of the chemicals noted above were used as received. All solutions were prepared with ultrapure water (laboratory water

DOI: 10.1021/acsami.9b01508
ACS Appl. Mater. Interfaces 2019, 11, 12880−12889

purifying device, Nanjing Qianyan Instrument Equipment Co., Ltd., China).

2.2. Preparation of the ZnO@PVA/KGM Nanofiber Membranes. *2.2.1. Preparation of the ZnO@PVA/KGM Solution for Electrospinning.* The PVA solution (10 wt %) was prepared by dissolving 10 g of PVA in 90 mL of ultrapure water and then stirred at 85 °C for 4 h. KGM (1 g) was dissolved in 9 mL of ultrapure water and stirred at room temperature for 1 h (1 wt % KGM solution). PVA/KGM solutions were obtained by mixing the PVA and KGM solutions in different weight ratios (9:1, 8:2, 7:3, 6:4, and 5:5) followed by stirring for 2 h at room temperature. Details of the optimization experiment are provided in the Supporting Information. PVA/KGM solutions (weight ratio 8:2) containing 0.06, 0.08, 0.1, 0.2, 0.4, and 0.6 wt % citric acid (CA) were prepared as well. The ZnO nanoparticles of different weight ratios (0, 0.5, 1.0, 1.5, and 2.0 wt %) were dispersed in ultrapure water and further mixed with PVA and KGM to form the composite precursor solution. All of the solutions were further stirred (ultrasonic stirring; 40 kHz) for 2 h at room temperature to form the homogeneously blended electrospinning solution.

2.2.2. Fabrication of ZnO@PVA/KGM Nanofiber Membranes by Electrospinning. The nanofiber membranes were fabricated using commercially available electrospinning equipment (FM1206, Beijing Future Material Scitech Co., Ltd., China). PVA/KGM solutions (see above) containing ZnO nanoparticles (0, 0.5, 1.0, 1.5, and 2.0 wt %) were prepared. Typically, ZnO@PVA/KGM dispersions were transferred into a 5 mL plastic syringe attached to a capillary tip with an inner diameter of 0.7 mm and pumped out at the rate of 0.66 mL h^{-1}. An electric potential of 18 kV was supplied to the metal needles to form charged liquid jets that, upon rapid evaporation of the solvent, turned into nanofibers on the collector of the instrument (the distance between the capillary tip and the fiber collector was 15 cm). All of the nanofibers were deposited on the nonwoven substrate (15 cm × 15 cm) that overlaid on a grounded metal roller (diameter of 12 cm) rotated at a speed of 50 rpm. To guarantee uniform membranes, the injection pump was set to move horizontally backward and forward at a speed of 20 cm min^{-1} over a distance of 2 cm. The temperature and relative humidity in the laboratory were 25 ± 2 °C and 40 ± 2%, respectively. After electrospinning, all of the samples were dried (vacuum drying at 60 °C for 1 h) to remove the residual solvent. Then, membranes were subsequently subjected to vacuum drying at 140 °C for 2 h to complete the esterification reaction (thermal cross-linking). After thermal cross-linking, esterification occurs between the hydroxyl groups of PVA and KGM and the carboxyl groups of CA (Figure 1a).

2.3. Resistance of PVA/KGM Nanofiber Membranes to Water. The pre-cross-linked membrane was cut into 2 × 2 cm^2, and the weight of the small film was measured; then, the membrane was immersed in 50 mL distilled water at room temperature and soaked for 24 h. After soaking for 24 h, the membrane was dried (vacuum freeze-drying, −48 °C, 12 h) and the weight of the membrane was measured. The degree of cross-linking can be quantitatively analyzed by the weight loss rate. The weight loss of the membranes, $W(\%)$, upon dispersing them in water was calculated from the equation below[32]

$$W(\%) = \frac{M_1 - M_2}{M_1} \times 100 \quad (1)$$

where M_1 is the initial weight of the membrane and M_2 is the weight of the membrane after immersing for 24 h in water and subsequently drying.

2.4. Air Filtration Tests. The filtration performance of the membranes was evaluated using an LZC-H filter tester (Huada Filter Technology Co., Ltd., China, details are provided in Figure S1). The detailed filtration measurements for the composite membrane are presented in the Supporting Information. The durability and reuse performance were determined by testing the membrane for more than 30 cycles and 300 min. A membrane (10 × 10 cm^2 effective area) was placed on the filter bracket. The filter tester made use of di-iso-octyl sebacate (DEHS) and neutral monodisperse NaCl particles as aerosol particles (diameter ranging from 300 nm to 10 μm). The neutralized NaCl and DEHS aerosol particles were transported, upward and downward, through the membranes.[12] A flow meter was used to adjust the air flow, which was set as 32 L min^{-1} in our experiments. The removal efficiency can be calculated by detecting the number of airborne particles in the upstream and downstream of the air flow, which could be calculated from the equation $\eta = 1 - \varepsilon_1/\varepsilon_2$, where ε_1 and ε_2 represent the quantities of aerosol particles in the downstream and upstream of the filter, respectively.[33] The pressure drop over the upstream and downstream sides of the membrane was measured by a flow gauge and two electronic pressure transmitters, as shown in Figure S1, Supporting Information. Each membrane was tested three times. The quality factor (QF), a widely used parameter to appraise the filtration performance of filters, was calculated by eq 2, where η is the removal efficiency of the membrane and Δp is the pressure drop over the membrane filters.

$$\mathrm{QF} = -\frac{\ln(1 - \eta)}{\Delta p} \quad (2)$$

2.5. Photocatalytic Activity Tests. It was aimed to investigate the role of the ZnO nanoparticles loaded on the electrospun membrane and their influence on the degradation of methyl orange (MO). Methyl orange (MO) solution (50 mL, 20 mg L^{-1}) was initially taken for the photocatalytic studies. The photocatalytic degradation of MO was carried out in a 100 mL cylindrical photoreactor. Upon irradiation, the light intensity equaled 83 mW cm^{-2} (solar simulator; 300 W xenon lamp, CEL-HXF300). The MO samples were collected every 5 min at the first 35 min and every 10 min afterward from the suspension and filtered by an MO-saturated Whatman filter to remove the catalyst before further analysis. Prior to irradiation, the solution was stirred in the dark for 120 min to achieve the adsorption−desorption equilibrium. The MO concentrations were measured by a UV−vis diffuse reflectance spectra spectrophotometer (UV-2600, Shimadzu, Japan) at the maximum absorption wavelength (λ) of 462 nm. The MO removal efficiency, $\varepsilon(\%)$, of photocatalytic degradation of MO was calculated using eq 3, where C_0 and C are the initial and final concentrations of the MO solution, respectively.

$$\varepsilon(\%) = \frac{C_0 - C}{C_0} \times 100\% \quad (3)$$

2.6. Testing the Antibacterial Activity of the ZnO@PVA/KGM Membranes. Agar solution was poured into a disposable sterile culture dish and allowed to solidify. A suspension of Gram-negative (*E. coli*) and Gram-positive (*Bacillus subtilis*) bacteria was uniformly applied on the agar plate, respectively. Electrospun nanofiber membranes were cut into circular films (diameter of 8 mm). The circular films were aseptically manipulated with sterile forceps and gently pressed to bring them into intimate contact with the solid medium. The culture dishes were subsequently incubated at 37 °C for 24 h. The antibacterial activity of the ZnO@PVA/KGM membranes was estimated from the area in which bacterial growth was inhibited (inhibition zone) using ImageJ.

2.7. Characterization. The surface morphology and EDS spectra of the membranes were studied by field-emission scanning electron microscopy (FE-SEM, S-4800, Hitachi Ltd., Japan). The surface of the ZnO-loaded filters was analyzed using an X-ray photoelectron spectrometer (XPS) (AXIS Ultra DLD, UK). The extent of cross-linking in the fibers was determined from Fourier transform infrared (FT-IR) spectra (Nicolet 8700 FT-IR spectrometer). The thermal stability of the membranes was evaluated with a thermal gravimetric analyzer (TGA Q5000-IR, TA Instruments). The mechanical properties were characterized by a Sans UTM6502 universal testing machine (Shenzhen, China). The leached quantity of the ZnO was analyzed by inductively coupled plasma atomic emission spectroscopy (ICP-MS, PerkinElmer Nixon 300X). Fluorescence photographs of the composite membranes were taken using a laser scanning confocal microscope (Carl Zeiss, LSM710). The pore size distribution was determined by a surface area and porosity analyzer at 77 K (Quantachrome BET instrument, Quantachrome Corporation).

DOI: 10.1021/acsami.9b01508
ACS Appl. Mater. Interfaces 2019, 11, 12880−12889

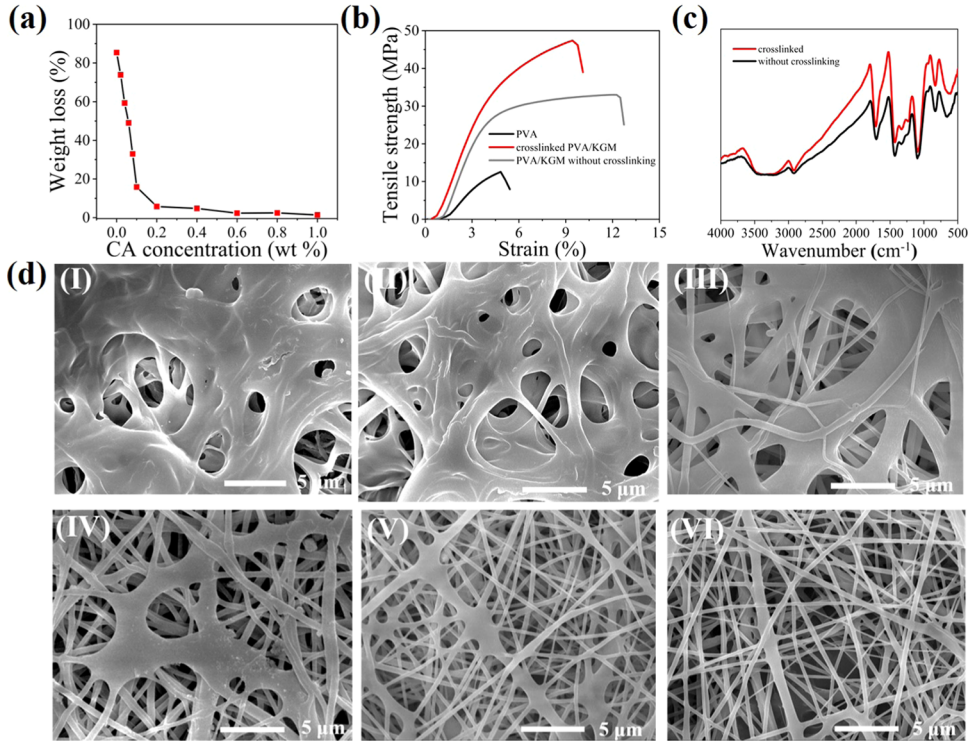

Figure 2. Water resistance of the thermally cross-linked PVA/KGM nanofiber membranes. (a) Weight loss of the membranes after 24 h of immersion in water; note that the CA concentration was varied. (b) Mechanical properties of the membranes. (c) FT-IR spectrum of the membranes before and after thermal cross-linking. (d) FE-SEM images of the membranes after 24 h in water. The CA concentration varied from 0.06 (I) to 0.08 (II), 0.1 (III), 0.2 (IV), 0.4 (V), and 0.6 (VI) wt %.

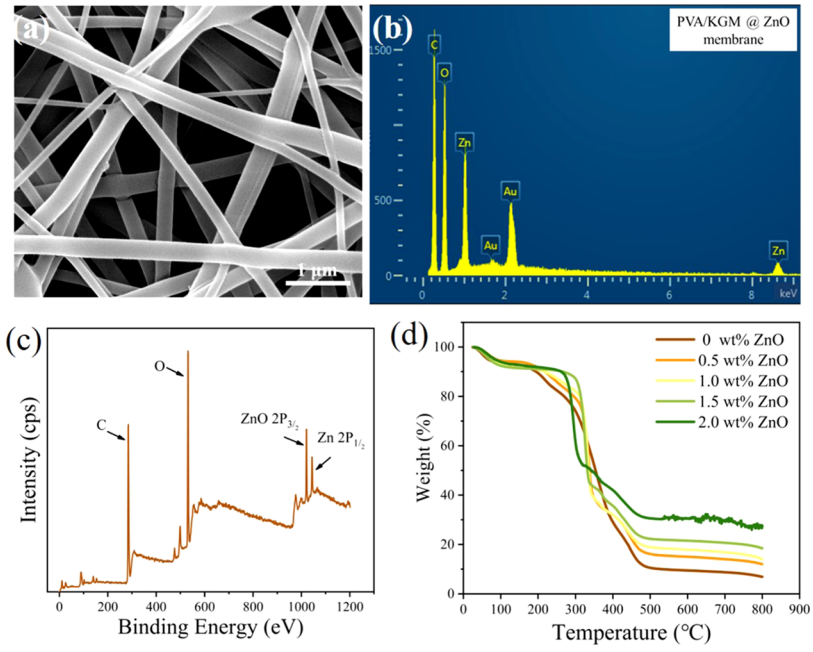

Figure 3. Characterization of the ZnO@PVA/KGM nanofiber membranes. (a) SEM image of a ZnO-loaded membrane. (b) EDS and (c) XPS images of ZnO@PVA/KGM nanofiber membranes (2.0 wt % ZnO). (d) TGA of membranes with different ZnO concentrations.

3. RESULTS AND DISCUSSION

3.1. Water Resistance of PVA/KGM Nanofibrous Membranes. As pure PVA nanofiber immediately dissolves when it comes in contact with water, incorporating it with plasticizers, cross-linking agents, or hybrids with other natural polymers can effectively improve the properties. Here, the nature-originated polymer KGM was selected to electrospun with the water-soluble polymer PVA to form the uniform nanofiber membrane in this work. CA as the cross-linking agent was added into the hybrid PVA/KGM solution. The optimum proportion of additives was determined by initial screening tests and a hydrolysis-resistant experiment (Supporting Information).

DOI: 10.1021/acsami.9b01508
ACS Appl. Mater. Interfaces 2019, 11, 12880−12889

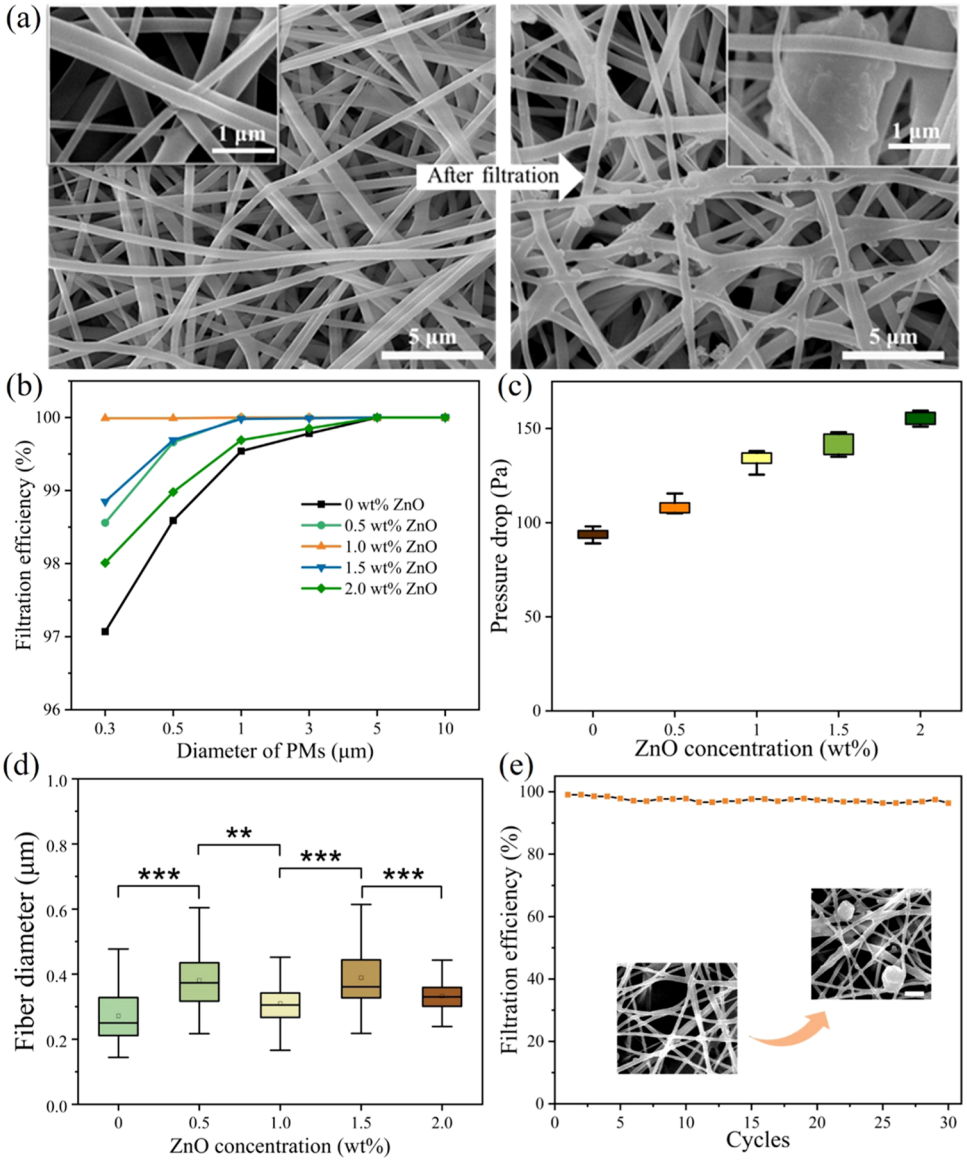

Figure 4. Filtration performance of the ZnO@PVA/KGM electrospun membranes (1.0 wt % ZnO). (a) SEM images of the nanofiber membrane before (left) and after (right) filtration. (b) Removal efficiency (η in eq 2) of the membranes varying in ZnO concentration (a constant air flow of 32 L min^{-1} was used). (c) Pressure drop measured over membranes loaded with different ZnO concentrations (the aerosol particle diameter in the experiments was 300 nm). (d) Diameter (distribution) of the fibers (as measured from EM images, using ImageJ software). (e) Removal efficiency of the membranes after multiple filtration cycles; SEM images of the membranes; the scale bar is 2 μm (*P < 0.05, **P < 0.01, ***P < 0.001).

Initial screening experiments with PVA/KGM solutions (varying in PVA/KGM composition) revealed that PVA/KGM solution with a weight ratio of 8:2 could generate uniform nanofibers (Table S1). Subsequently, PVA/KGM-CA solutions (varying in CA concentration) were electrospun into fibers. These nanofibers were then thermally treated to complete the cross-linking process. Thus obtained membranes were immersed in water for 24 h and subsequently dried. Figure 2a shows that the weight loss of the membranes (upon dispersing them in water) could be significantly prevented when a sufficiently high concentration of CA was used (0.6 wt %). Figure 2d shows that the membranes with low amounts of CA became severely swollen and deformed when immersed in water. Using higher amounts of CA significantly improved the resistance to water; with 0.6 wt % CA, the morphology of the nanofiber membranes did no longer change after being in contact with water for 24 h, as shown in Figure 2d(I–VI).

Upon thermal treatment, esterification should occur between the hydroxyl groups of PVA and KGM and the carboxyl groups of CA (Figure 1) after the 140 °C heat treatment, which could readily overcome the inherent hydroinstability, thus changing a previously water-soluble material to an insoluble material. FT-IR measurements (Figure 2c) indeed confirmed the thermal cross-linking of the PVA/KGM-CA nanofiber membranes. The large bands at around 3320 cm^{-1} correspond to the -OH stretching of intramolecular and intermolecular hydrogen bonds; bands at 2940 and 852 cm^{-1} are the backbones of $-CH_2$ symmetric stretching vibration and out-of-plane twisting, respectively; the small bands at 1097 cm^{-1} correspond to "-C-O". It can be seen that the stretching vibration of "-C═O" (1700 cm^{-1}) becomes stronger after thermal cross-linking, which means that the "-C═O" stretching vibration (1720 cm^{-1}) is normally shifted to the right through esterification. Also, the absorption peak

DOI: 10.1021/acsami.9b01508
ACS Appl. Mater. Interfaces 2019, 11, 12880–12889

(at 3400 cm^{-1}) of -OH groups becomes weak, all proving that the esterification cross-linking reaction was successfully conducted. Furthermore, the mechanical properties of the pure PVA membrane and PVA/KGM composite membrane before and after cross-linking were characterized, as shown in Figure 2b. It is found that the KGM itself could obviously enhance the mechanical strength of the membrane. After the cross-linking treatment, the mechanical performance of the membrane significantly improved, which further confirmed that the cross-linking process not only endows the membrane with water resistance but also improves the mechanical properties.

3.2. PVA/KGM Nanofiber Membranes Loaded with ZnO Nanoparticles. We applied SEM to visualize the surface morphology of ZnO@PVA/KGM membranes. As Figure 3a shows, electrospun nanofibers were uniformly distributed, whereas ZnO nanoparticles were not observed; it suggests that, due to their small size (30 ± 10 nm), the ZnO nanoparticles were encapsulated by the nanofibers (diameter >100 nm; see further). Meanwhile, as shown in Figure 3b and Table S3, we took advantage of energy-dispersive spectrometry (EDS) to determine the characteristics of the ZnO nanoparticles on the fibers; the results confirmed that the ZnO nanoparticles were successfully loaded in the membrane. Surface characterization of the ZnO@PVA/KGM composite membrane was analyzed by an X-ray photoelectron spectrometer (XPS). Figure 3c shows that two well-separated peaks of ZnO $2p_{3/2}$ and Zn $2p_{1/2}$ could be observed at 1021 and 1044 eV, respectively. These proved that the ZnO particles were relatively stable in oxidation. Fluorescence photographs were obtained by a laser scanning confocal microscope. As shown in Figure S2a,b, the ZnO nanoparticles loaded in the fibers endow the whole fiber to emit a bright fluorescence, indicating that ZnO nanoparticles were attached and dispersed uniformly in the fiber since the fluorescence is continuous and uniform. The combination of both ZnO nanoparticles and the nanofibers was studied by a leaching test (Supporting Information). The ICP measurement results (Table S2) showed that the concentrations of leached ZnO in water were relatively low after continuous shaking, indicating that there are good attachments between the ZnO nanoparticles and the nanofibers. Based on these results, it could be confirmed that the electrospun process enables the direct formation of densely structured ZnO particles onto the filter fibers. The thermal stabilities of ZnO nanoparticle-loaded nanofibrous membrane were investigated by a thermogravimetric analyzer (TGA) from 30 °C to 800 °C (under a nitrogen atmosphere). As shown in Figure 3d, there is little change in weight before 100 °C, which may be due to the slight dehydration of PVA and KGM under heating conditions. Degradation of the ZnO@PVA/KGM nanofibrous membrane started around 300 °C followed by a fast degradation at higher temperatures, and then, the curve of weight percentage shows a fast drop. This may be attributed to the degradation of the polymer framework. With the increase of temperature, the weight percentage decreased slowly after 500 °C and tended to be stabilized. Interestingly, we found that the thermal stability of these ZnO@PVA/KGM composite electrospun nanofibrous membranes increases with the increase of ZnO amount, which means that the ZnO@PVA/KGM composite membranes is seized of a good thermal stability at temperature up to 300 °C, which can be applicable in some middle-temperature environment conditions.

3.3. Filtration Performances of ZnO@PVA/KGM Nanofibrous Membranes. The SEM images presented in Figure 4a show a typical surface morphology of the ZnO@PVA/KGM nanofibrous membrane (1.0 wt % ZnO) before and after a filtration test. To further enhance the filtration performance of the blend PVA/KGM fibrous filter, the nanosized ZnO particles were added into the PVA/KGM system by electrospinning the mixture of ZnO and PVA/KGM solution to form a fibrous membrane. To explore the role of ZnO nanoparticles loaded on nanofiber membranes, the filtration efficiency of the green electrospun nanofiber membrane with different ZnO concentrations for various particle diameters from 0.3 to 10 μm was systematically investigated under the designed air flow of 32 L min^{-1}, as shown in Figure 4b and Table S4. The filtration efficiency showed an improved trend with the increase of the ZnO concentration, which could be attributed to the increased surface roughness and specific surface area that played a dominant role in the particle intercept of the ZnO@PVA/KGM membrane. Since filters always show relative low filtration efficiency for submicron particles, here, the filtration efficiency mentioned is for 0.3 μm particles. Although the membrane without ZnO could achieve a high removal efficiency level of >97%, with the increasing ZnO content from 0 to 1.0 wt %, the filtration efficiency further increases from 97.07 to 99.99%. Meanwhile, we found that its pressure drop increased accordingly from 89.0 to 130.0 Pa, as shown in Figure 4c and Table S4. Interestingly, the filtration efficiency further decreased to 98.01% (pressure drop increased to 158 Pa) when the ZnO concentration was increased from 1.0 to 2.0 wt %, which could be ascribed to the poor spinnability of the precursor solution caused by high ZnO concentration. This suggests an unreasonable tradeoff design for practical applications: slightly enhanced efficiency at the expense of hugely increased pressure drop. Based on the QF value (Figure S3), the nanofiber membranes that contain 1.0 wt % ZnO were selected as, being the most optimum condition, these take both the filtration efficiency (99.99%) and pressure drop (130 Pa) into consideration. It is worth noting that the filtration efficiency almost approached to 100% when the diameter of the particles is larger than 1 μm, furthermore, which could maintain 100% filtration efficiency for particles with diameters of 5 and 10 μm (PM_{10}).

We further investigated the pore size and pore distribution of the composite membranes with ZnO contents of 0, 0.5, 1.0, 1.5, and 2.0 wt % (Figure S4). The ZnO@PVA/KGM membranes showed the pore size distribution in the range of 0.6−25 nm and a single pore distribution peak, thus confirming that the membranes possessed a uniform and relatively narrow pore distribution. It is worth noting that the pore size decreased with the increasing ZnO content. Moreover, the cumulative pore size distributions of membranes with 1 wt % ZnO presented that most of the pores are concentrated between 2.4 and 4.9 nm. SEM imaging also revealed that the diameter (distribution) of the fibers depended on the ZnO concentration. A further systematic investigation of the fiber diameters was carried out by ImageJ software, and the diameter distributions are presented in Figure S6. To analyze that the diameter distribution varied with the ZnO concentration, the fiber diameters of different ZnO concentrations were analyzed by the mathematical statistics software SPSS (Supporting Information), and the results are presented in the box chart (Figure 4d), where data points are the means and the standard deviations of samples.

DOI: 10.1021/acsami.9b01508
ACS Appl. Mater. Interfaces 2019, 11, 12880−12889

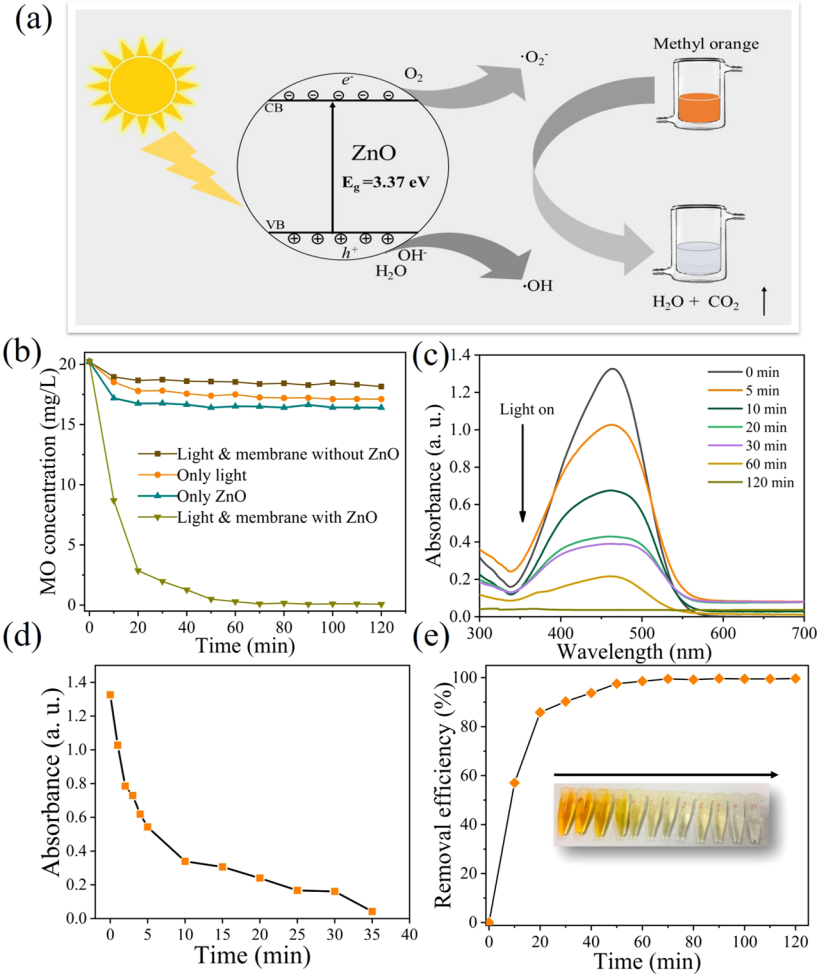

Figure 5. Photocatalytic activity of the ZnO-loaded membranes. (a) Illustration of the mechanism of the photocatalytic degradation of methyl orange. (b) MO concentration as a function of time under various conditions, i.e., exposing the MO solution to, respectively, light (only), ZnO-loaded membranes (only), light and a membrane without ZnO, and the combination of light and ZnO-loaded membranes. (c) Adsorption spectra of MO solutions exposed to ZnO-loaded membranes and light. (d) Absorption (λ = 464 nm) of the MO solution as a function of time. (e) MO removal efficiency of the membrane as a function of time; the inset shows the gradual decoloring of the MO solution.

Results turned out that there is a significant difference between different ZnO concentrations. Compared to the ZnO@PVA/KGM (1.0 wt %) membranes, the fibers with the other percentages of ZnO have a large diameter size in a much broad diameter distribution. This further strongly confirmed the highest filtration efficiency and the relatively low pressure drop were found in the 1.0 wt % ZnO composite membrane.

To further investigate the reuse performance and durability of the ZnO-loaded hybrid PVA/KGM electrospun nanofiber membrane, the filtration efficiency of the membrane (1.0 wt % ZnO) was tested for 30 cycles (Figure 4e) and 300 min (Figure S5). The membrane could maintain more than 97% filtration efficiency even after 150 min (Figure S5). Obviously, the ZnO@PVA/KGM nanofibrous membrane could be reused for as many as 30 cycles with the filtration efficiency maintained more than 98% for 0.3 μm particles (still maintain 100% for 5 and 10 μm particles). As the inset SEM images shows in Figure 4e, the particulate matters were adhered closely to the fibers in the surface of the filtration membrane. This phenomenon can be explained by that the larger particles were intercepted by the fibers during the filtration process, while the few extremely small ones may be crashed into the porous nanofiber and tightly adhered by virtue of the van der Waals force.[34]

3.4. Photocatalytic Activity of ZnO@PVA/KGM Nanofiber Membranes. ZnO has been proven to be efficient for photocatalysis (band gap 3.37 eV at room temperature).[35,36] The photocatalytic degradation mechanism of ZnO is illustrated in Figure 5a; when ZnO is irradiated by photons with an energy level exceeding its band gap, the energy excites electrons (e^-) from the valence band to the conduction band and holes (h^+) are generated in the valence band; strong oxidant hydroxyl radical ($^\bullet$OH) can be generated by the reaction between the photogenerated valence band holes and water (H_2O) or hydroxyl ions (OH^-), adsorbed on the surface of the catalyst. The photogenerated electrons in the conduction band may react with oxygen (O_2) to form the superoxide ions ($^\bullet O_2^-$) that can further react with water to produce hydrogen peroxide (H_2O_2) and hydroxyl ions (OH^-). The degradation of the organic dye can be realized through the reaction with hydroxyl radicals ($^\bullet$OH) or a direct attack from the valence band holes.

The photocatalytic performances of ZnO-loaded PVA/KGM electrospun membranes were evaluated from the reduction of MO, which is a typical highly colored, nonbiodegradable, and

DOI: 10.1021/acsami.9b01508
ACS Appl. Mater. Interfaces 2019, 11, 12880−12889

toxic refractory organic dye. Photocatalysis experiments were carried out by nanofiber membranes with and without ZnO nanoparticles (control samples) using a 300 W xenon lamp. It is worth noting that the membrane used here was loaded with 2.0 wt % ZnO, expect where noted. The samples were collected from the reactor at various exposure times. Prior to illumination, the solution was kept in the dark for 120 min and stirred to reach an adsorption−desorption equilibrium. Absorption measurements on MO solutions revealed that exposing the MO solutions (during 2 h) to, respectively, light and a membrane without ZnO, light (only), ZnO (only), and the combination of light and ZnO-loaded membranes decreased 9, 15, 17, and 98% of their initial concentration, respectively, clearly indicating that the cotreatment with the ZnO-loaded membrane and visible light significantly promoted the degradation (Figure 5b). The typical UV−vis spectra of the MO solutions are presented in Figure 5c; a decrease in the peak intensity with time shows that the MO dye was efficiently decreased and the catalysts were photoactive. To further investigate the changes of the MO solutions, the max absorbance of MO in the typical UV−vis spectra is presented in Figure 5d. It was obvious that the MO concentration was significantly reduced and the absorbance of MO almost tended to 0 after 35 min of light irradiation. As shown in Figure 5e, the MO color obviously changed after light irradiation and the degradation efficiency almost reached 98% after 120 min by virtue of solar irradiation and photocatalyst ZnO. Finally, we can conclude that nanosized ZnO particles could noticeably enhance the photocatalytic activity of the composite membranes.

3.5. Antibacterial Activity of the ZnO@PVA/KGM Membranes. The active ZnO nanoparticles possess good biocompatibility, superior safety, and long-term effect. ZnO could show excellent antibacterial properties in the absence of light, even at low concentrations. Here, the antibacterial activities of the ZnO-loaded PVA/KGM electrospun nanofibrous membranes were investigated by both *E. coli* and *Bacillus subtilis*. As shown in Figure 6a,b, the ZnO@PVA/KGM nanofibrous membranes showed obvious antibacterial activities against both *E. coli* and *Bacillus subtilis* compared to the control samples (without ZnO nanoparticles). A general trend could be obtained; the antibacterial performance could be enhanced significantly with the increase of the ZnO concentration. To quantitatively analyze the antibacterial performance of the electrospun ZnO-loaded nanofiber membrane, the diameter of the bacteriostatic ring was measured and analyzed, as shown in Figure 6c. The highest antibacterial activity for both *E. coli* and *Bacillus subtilis* was found in 1.0 and 2.0 wt % ZnO@PVA/KGM, respectively. However, we interestingly found that when the ZnO content is greater than 1.0 wt %, the antibacterial activity for *E. coli* did not increase but decreased. This can be explained by the fact that the ZnO nanoparticles could be uniformly dispersed over the membrane surface when the ZnO concentration was 1.0 wt %. However, when the concentration was increased to more than 1.0 wt % and reached a higher value, the spinnability of the blend solutions reduced markedly and the ZnO particles gathered into clusters and adhered into the fibrous membranes, randomly. Compared to the membrane uniformly dispersed with ZnO nanoparticles, the membrane with random ZnO clusters (may be somewhere without) has shown lower antibacterial activity and may be entirely persuasive.

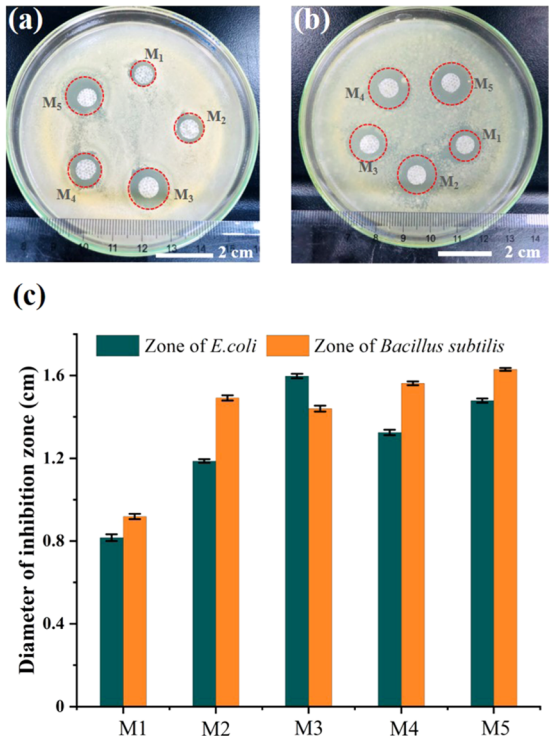

Figure 6. Antibacterial activity of ZnO@PVA/KGM nanofiber membranes against (a) *E. coli* and (b) *Bacillus subtilis*. M1−M5 correspond to membranes loaded with varying amounts of ZnO (0, 0.5, 1.0, 1.5 and 2.0 wt %, respectively). (c) Diameter of the inhibition zones as a function of the weight percentage of ZnO in the membranes.

4. CONCLUSIONS

We proposed a new method of preparation of ecofriendly cross-linked blend PVA/KGM electrospun nanofiber membranes loaded with ZnO nanoparticles. The strategy of thermal cross-linking significantly improved the water resistance and mechanical properties of the polyhydroxyl water-soluble polymer. Besides, the introduction of active ZnO nanoparticles not only remarkably improves the filtration efficiency but also endows the ZnO@PVA/KGM membrane with photocatalytic activity and antibacterial activity. The composite membrane presents a superior filtration efficiency to commercial HEPA filters, a high photocatalytic degradation efficiency of more than 98% and a superior antibacterial activity against both Gram-negative (*E. coli*) and Gram-positive bacteria (*Bacillus subtilis*). For the above-mentioned superiorities, we expect that such multifunctional nanofiber membranes will be greatly helpful for reducing environmental contamination by the air filtration systems and photocatalytic degradation features as well as the antibacterial properties.

■ ASSOCIATED CONTENT

Supporting Information

The Supporting Information is available free of charge on the ACS Publications website at DOI: 10.1021/acsami.9b01508.

Initial screening experiments and hydrolysis-resistant tests, leaching test, filtration measurement of the fibrous membrane, statistical analysis, characterization of pore size and its distribution, optical photograph and schematic diagram of the filtration tester, confocal microscopy images of the electrospun membranes, QF

DOI: 10.1021/acsami.9b01508
ACS Appl. Mater. Interfaces 2019, 11, 12880−12889

of the ZnO@PVA/KGM nanofiber membranes, pore size distribution of the composite membranes, filtration performance of the composite membrane over time, FE-SEM images of ZnO@PVA/KGM composite membranes and the diameter distribution of the fibers, EDS data of the composite membrane with 2.0 wt % ZnO nanoparticles, leaching test results of ZnO nanoparticles, and filtration performance of the composite membranes (PDF)

AUTHOR INFORMATION

Corresponding Authors

*E-mail: ranhua.xiong@gmail.com (R.X.).
*E-mail: huangchaobo@njfu.edu.cn (C.H.).

ORCID

Jiandu Lei: 0000-0002-1432-0588
Jingquan Han: 0000-0002-1306-5431
Stefaan De Smedt: 0000-0002-8653-2598
Chaobo Huang: 0000-0003-3484-0545

Notes

The authors declare no competing financial interest.

ACKNOWLEDGMENTS

The National Natural Science Foundation of China (Nos. 21774060 and 31770609), the National Key R&D Program of China (2017YFF0207800), the Jiangsu Key Lab of Biomass-based Energy and Materials (JSBEM2016011), the State Key Laboratory for Mechanical Behavior of Materials (20171914), the Priority Academic Program Development of Jiangsu Higher Education Institutions (PAPD), the Top-notch Academic Programs Project of Jiangsu Higher Education Institutions (TAPP), and the Natural Science Key Project of the Jiangsu Higher Education Institutions (16KJA220006) are acknowledged with gratitude. We also thank Advanced Analysis & Testing Center, Nanjing Forestry University for SEM characterization.

REFERENCES

(1) Brunekreef, B.; Holgate, S. T. Air pollution and health. *Lancet* **2002**, *360*, 1233−1242.

(2) Bardouki, H.; Liakakou, H.; Economou, C.; Sciare, J.; Smolík, J.; Ždímal, V.; Eleftheriadis, K.; Lazaridis, M.; Dye, C.; Mihalopoulos, N. Chemical composition of size-resolved atmospheric aerosols in the eastern Mediterranean during summer and winter. *Atmos. Environ.* **2003**, *37*, 195−208.

(3) Nel, A. Air Pollution-Related Illness: Effects of Particles. *Science* **2005**, *308*, 804−806.

(4) Mahowald, N. Aerosol indirect effect on biogeochemical cycles and climate. *Science* **2011**, *334*, 794−796.

(5) Horton, D. E.; Skinner, C. B.; Singh, D.; Diffenbaugh, N. S. Occurrence and persistence of future atmospheric stagnation events. *Nat. Clim. Change* **2014**, *4*, 698−703.

(6) Zuo, F.; Zhang, S.; Liu, H.; Fong, H.; Yin, X.; Yu, J.; Ding, B. Free-Standing Polyurethane Nanofiber/Nets Air Filters for Effective PM Capture. *Small* **2017**, *13*, No. 1702139.

(7) Xu, J.; Liu, C.; Hsu, P.-C.; Liu, K.; Zhang, R.; Liu, Y.; Cui, Y. Roll-to-Roll Transfer of Electrospun Nanofiber Film for High-Efficiency Transparent Air Filter. *Nano Lett.* **2016**, *16*, 1270−1275.

(8) Liu, C.; Hsu, P.-C.; Lee, H.-W.; Ye, M.; Zheng, G.; Liu, N.; Li, W.; Cui, Y. Transparent air filter for high-efficiency PM2.5 capture. *Nat. Commun.* **2015**, *6*, No. 6205.

(9) Lv, D.; Zhu, M.; Jiang, Z.; Jiang, S.; Zhang, Q.; Xiong, R.; Huang, C. Green Electrospun Nanofibers and Their Application in Air Filtration. *Macromol. Mater. Eng.* **2018**, *303*, No. 1800336.

(10) Zhang, S.; Liu, H.; Yin, X.; Yu, J.; Ding, B. Anti-deformed Polyacrylonitrile/Polysulfone Composite Membrane with Binary Structures for Effective Air Filtration. *ACS Appl. Mater. Interfaces* **2016**, *8*, 8086−8095.

(11) Sambaer, W.; Zatloukal, M.; Kimmer, D. 3D modeling of filtration process via polyurethane nanofiber based nonwoven filters prepared by electrospinning process. *Chem. Eng. Sci.* **2011**, *66*, 613−623.

(12) Zhu, M.; Hua, D.; Pan, H.; Wang, F.; Manshian, B.; Soenen, S. J.; Xiong, R.; Huang, C. Green electrospun and crosslinked poly(vinyl alcohol)/poly(acrylic acid) composite membranes for antibacterial effective air filtration. *J. Colloid Interface Sci.* **2018**, *511*, 411−423.

(13) Wan, H.; Wang, N.; Yang, J.; Si, Y.; Chen, K.; Ding, B.; Sun, G.; El-Newehy, M.; Al-Deyab, S. S.; Yu, J. Hierarchically structured polysulfone/titania fibrous membranes with enhanced air filtration performance. *J. Colloid Interface Sci.* **2014**, *417*, 18−26.

(14) Wang, Z.; Zhao, C.; Pan, Z. Porous bead-on-string poly(lactic acid) fibrous membranes for air filtration. *J. Colloid Interface Sci.* **2015**, *441*, 121−129.

(15) Li, Q.; Xu, Y.; Wei, H.; Wang, X. An electrospun polycarbonate nanofibrous membrane for high efficiency particulate matter filtration. *RSC Adv.* **2016**, *6*, 65275−65281.

(16) Zhang, R.; Liu, C.; Hsu, P. C.; Zhang, C.; Liu, N.; Zhang, J.; Lee, H. R.; Lu, Y.; Qiu, Y.; Chu, S.; Cui, Y. Nanofiber Air Filters with High-Temperature Stability for Efficient PM2.5 Removal from the Pollution Sources. *Nano Lett.* **2016**, *16*, 3642−3649.

(17) Nthunya, L. N.; Masheane, M. L.; Malinga, S. P.; Nxurnalo, E. N.; Barnard, T. G.; Kao, M.; Tetana, Z. N.; Mhlanga, S. D. Greener Approach To Prepare Electrospun Antibacterial beta-Cyclodextrin/Cellulose Acetate Nanofibers for Removal of Bacteria from Water. *ACS Sustainable Chem. Eng.* **2017**, *5*, 153−160.

(18) Pangon, A.; Saesoo, S.; Saengkrit, N.; Ruktanonchai, U.; Intasanta, V. Multicarboxylic acids as environment-friendly solvents and in situ crosslinkers for chitosan/PVA nanofibers with tunable physicochemical properties and biocompatibility. *Carbohydr. Polym.* **2016**, *138*, 156−165.

(19) Zhang, B.; Yan, X.; He, H.-W.; Yu, M.; Ning, X.; Long, Y.-Z. Solvent-free electrospinning: opportunities and challenges. *Polym. Chem.* **2017**, *8*, 333−352.

(20) Jiang, S.; Hou, H.; Agarwal, S.; Greiner, A. Polyimide Nanofibers by "Green" Electrospinning via Aqueous Solution for Filtration Applications. *ACS Sustainable Chem. Eng.* **2016**, *4*, 4797−4804.

(21) Giebel, E.; Mattheis, C.; Agarwal, S.; Greiner, A. Chameleon Nonwovens by Green Electrospinning. *Adv. Funct. Mater.* **2013**, *23*, 3156−3163.

(22) Nicosia, A.; Gieparda, W.; Foksowicz-Flaczyk, J.; Walentowska, J.; Wesolek, D.; Vazquez, B.; Prodi, F.; Belosi, F. Air filtration and antimicrobial capabilities of electrospun PLA/PHB containing ionic liquid. *Sep. Purif. Technol.* **2015**, *154*, 154−160.

(23) Celebioglu, A.; Uyar, T. Green and one-step synthesis of gold nanoparticles incorporated into electrospun cyclodextrin nanofibers. *RSC Adv.* **2013**, *3*, 10197−10201.

(24) Choi, D. Y.; Jung, S.-H.; Song, D. K.; An, E. J.; Park, D.; Kim, T.-O.; Jung, J. H.; Lee, H. M. Al-Coated Conductive Fibrous Filter with Low Pressure Drop for Efficient Electrostatic Capture of Ultrafine Particulate Pollutants. *ACS Appl. Mater. Interfaces* **2017**, *9*, 16495−16504.

(25) Zhang, Y.; Yuan, S.; Feng, X.; Li, H.; Zhou, J.; Wang, B. Preparation of Nanofibrous Metal−Organic Framework Filters for Efficient Air Pollution Control. *J. Am. Chem. Soc.* **2016**, *138*, 5785−5788.

(26) Zhu, J.; Lin, X.; Zhang, Z.; Luo, X. Preparation and characterization of KGM-g-St/BA fibers and core/shell PCL/KGM-g-St/BA fibers. *RSC Adv.* **2015**, *5*, 24975−24983.

(27) Wang, L.; Mu, R.-J.; Yuan, Y.; Gong, J.; Ni, Y.; Wang, W.; Pang, J. Novel nanofiber membrane fabrication from konjac glucomannan and polydopamine via electrospinning method. *J. Sol-Gel Sci. Technol.* **2018**, *85*, 253−258.

DOI: 10.1021/acsami.9b01508
ACS Appl. Mater. Interfaces 2019, 11, 12880−12889

(28) Özgür, U.; Alivov, Y. I.; Liu, C.; Teke, A.; Reshchikov, M. A.; Dogan, S.; Avrutin, V.; Cho, S. J.; Morkoc, H. A comprehensive review of ZnO materials and devices. *J. Appl. Phys.* **2005**, *98*, No. 041301.
(29) Ibrahim, N. A.; Eid, B. M.; El-Aziz, E. A.; Abou Elmaaty, T. M.; Ramadan, S. M. Multifunctional cellulose-containing fabrics using modified finishing formulations. *RSC Adv.* **2017**, *7*, 33219−33230.
(30) Ibrahim, N. A.; Eid, B. M.; El-Aziz, E. A.; Elmaaty, T. M. A.; Ramadan, S. M. Loading of chitosan − Nano metal oxide hybrids onto cotton/polyester fabrics to impart permanent and effective multifunctions. *Int. J. Biol. Macromol.* **2017**, *105*, 769−776.
(31) Ibrahim, N. A.; Eid, B. M. In *Handbook of Textile Effluent Remediation*; Yusuf, M., Eds.; Pan Stanford: New York, 2018; Chapter 7, pp 185−202.
(32) Sheng, J.; Zhang, M.; Xu, Y.; Yu, J.; Ding, B. Tailoring Water-Resistant and Breathable Performance of Polyacrylonitrile Nanofibrous Membranes Modified by Polydimethylsiloxane. *ACS Appl. Mater. Interfaces* **2016**, *8*, 27218−27226.
(33) Zhao, X.; Li, Y.; Hua, T.; Jiang, P.; Yin, X.; Yu, J.; Ding, B. Low-Resistance Dual-Purpose Air Filter Releasing Negative Ions and Effectively Capturing PM2.5. *ACS Appl. Mater. Interfaces* **2017**, *9*, 12054−12063.
(34) Zhu, M.; Han, J.; Wang, F.; Shao, W.; Xiong, R.; Zhang, Q.; Pan, H.; Yang, Y.; Samal, S. K.; Zhang, F.; Huang, C. Electrospun Nanofibers Membranes for Effective Air Filtration. *Macromol. Mater. Eng.* **2017**, *302*, No. 1600353.
(35) Sun, J.-X.; Yuan, Y.-P.; Qiu, L.-G.; Jiang, X.; Xie, A.-J.; Shen, Y.-H.; Zhu, J.-F. Fabrication of composite photocatalyst g-C3N4−ZnO and enhancement of photocatalytic activity under visible light. *Dalton Trans.* **2012**, *41*, 6756−6763.
(36) Kansal, S. K.; Singh, M.; Sud, D. Studies on photodegradation of two commercial dyes in aqueous phase using different photocatalysts. *J. Hazard. Mater.* **2007**, *141*, 581−590.

DOI: 10.1021/acsami.9b01508
ACS Appl. Mater. Interfaces 2019, 11, 12880−12889